

# QUANTUM DOT SOLAR CONCENTRATORS AND MODULES

A. J. Chatten<sup>1</sup>, K. W. J. Barnham<sup>1</sup>, B. F. Buxton<sup>2</sup>, N. J. Ekins-Daukes<sup>3</sup>, M. A. Malik<sup>4</sup>

<sup>1</sup>Physics Department, Imperial College, London, SW7 2BW, U.K.

<sup>2</sup>Computer Science Department, U.C.L., London, WC1E 6BT, U.K.

<sup>3</sup>Toyota Technological Institute, Nagoya, 468-8511, Japan.

<sup>4</sup>Chemistry Department, University of Manchester, Manchester, M13 9PL, U.K.

**ABSTRACT:** The luminescent properties of core-shell quantum dots (QDs) are being exploited in an unconventional solar concentrator module which promises to reduce the cost of photovoltaic electricity. Luminescent solar collectors have advantages over geometric concentrators in that tracking is unnecessary and both direct and diffuse radiation can be collected. However, development has been limited by the performance of luminescent dyes. We present experimental and theoretical results with a novel system in which the dyes are replaced by quantum dots. We have developed self-consistent thermodynamic models for planar concentrators and modules and find that these three-dimensional flux models show excellent agreement with experiment.

**Keywords:** Concentrators, Modelling, Quantum Dots

## 1 INTRODUCTION

The luminescent planar solar concentrator [1] was originally proposed in the late 1970s. It consisted of a transparent sheet doped with appropriate organic dyes. Sunlight is absorbed by the dye and then re-radiated isotropically, ideally with high quantum efficiency (QE) and trapped in the sheet by internal reflection. A stack of sheets doped with different dyes [1] can separate the light, and solar cells can be chosen to match the different luminescent wavelengths to convert the trapped light at the edge of the module.

Advantages over geometric concentrators include that expensive solar tracking is unnecessary and that both direct and diffuse radiation can be collected. However, the development of this promising concentrator was limited by the stringent requirements on the luminescent dyes, namely high QE, suitable absorption spectra and red-shifts and stability under illumination [2].

## 2 THE QUANTUM DOT CONCENTRATOR (QDC)

We have recently proposed a novel concentrator [3] in which the dyes are replaced by quantum dots (QDs). The first advantage of the QDs over dyes is the ability to tune the absorption threshold simply by choice of dot diameter. Secondly, high luminescence quantum efficiency has been observed. CdSe/CdS heterostructure dots have demonstrated luminescence quantum yields above 80% at room temperature [4]. Thirdly, since they are composed of crystalline semiconductor, the dots should be inherently more stable than dyes.

However, absorption losses in the host material and re-absorption limit the efficiency of the QDC. Our thermodynamic models [5,6] allow us to investigate quantitatively the distribution of dot diameters, doping density and geometry that minimise these sources of absorption losses.

## 3 THERMODYNAMIC MODELS

Our thermodynamic model [5] was developed by applying a detailed balance argument to relate the absorbed light to the spontaneous emission using self-consistent three-dimensional (3D) fluxes. The model is derived by applying the method of Schwarzschild and

Milne [7], in which the angular dependence of the radiative intensity described by Chandrasekhar's general three dimensional transfer equation [8] is ignored and the radiation is considered as consisting simply of forward (+) and backward (-) streams. We have extended this approach to streams parallel to the  $x$ ,  $y$ , and  $z$  axes of a concentrator and apply appropriate reflection boundary conditions to the radiation depending on whether it falls within the escape cone or the solid angle of total internal reflection.

The model allows for: (i) a significant fraction of the incident flux to be absorbed by the sheet, (ii) spectral overlap of the incident radiation with the luminescence, (iii) re-absorption of radiation emitted into the escape cone, and (iv) losses due to absorption in the host material, all of which could not be accounted for in earlier models [9]. Comparison with measurements on CdSe/CdS QDs in acrylic and organic dyes in perspex [6] show that the 3D flux model can predict both the room temperature red-shift and the total flux escaping each surface, providing a tool for optimisation of the QDC.

Here, we extend the model to concentrator modules, which are comprised of a slab with a solar cell bonded to one edge. This requires modifications to the model for concentrator slabs [5,6] and is presented here together with experimental results on both slabs and modules. The model provides equations from which the photon chemical potential as a function of position within a finite slab of material may be determined by iteration.

## 4 3D FLUX MODEL FOR A MODULE

We consider a finite slab of material of thickness  $D$  in the  $z$  direction, length  $L$  in the  $x$  direction and width  $W$  in the  $y$  direction, uniformly illuminated on the top surface with a solar cell covering and bonded to the right-hand surface. We assume that all of the narrow band luminescence propagating into the solar cell is absorbed such that we only need to consider reflection at the slab/glue/cell interface.

In addition to the forward and backward radiation streams, we also distinguish what happens when the direction of propagation,  $\theta$ , is greater or less than the critical angle  $\theta_c$ . Escaping photons with  $\theta < \theta_c$  and trapped photons with  $\theta > \theta_c$  are treated as separate streams [5].

#### 4.1 Escaping fluxes

Integrating the radiative transfer equation over the escape cones in each co-ordinate direction produces two differential equations [6] for the luminescent escaping fluxes propagating in the positive and negative directions:

$$\mp \frac{\partial I_{x,y,z}^{(\pm)}}{\partial x,y,z} = \lambda_a I_{x,y,z}^{(\pm)} - \frac{\Omega_c}{4\pi} \lambda_e B \quad (1)$$

In Eqn. 1,  $I_x^{(\pm)}$ ,  $I_y^{(\pm)}$  and  $I_z^{(\pm)}$  are the escaping luminescent fluxes propagating within the slab in the positive and negative  $x$ ,  $y$  and  $z$  directions respectively, and,  $\lambda_a$  and  $\lambda_e$  are defined by:

$$\lambda_a = \frac{N\sigma_a(\nu)}{\cos^2(\theta_c/2)} \quad \lambda_e = \frac{N\sigma_e(\nu)}{\cos^2(\theta_c/2)} \quad (2)$$

Here,  $N$  is the density of luminescent centres,  $\sigma_a(\nu)$  is the absorption cross section of the slab material comprising a transparent medium with absorption cross section  $\sigma_b(\nu)$  within which is uniformly distributed the luminescent species with cross section  $\sigma_e(\nu) = \sigma_a(\nu) - \sigma_b(\nu)$ . The luminescent brightness,  $B$ , of a radiation field in equilibrium with the electronic degrees of freedom of the absorbing species is given by

$$B(\nu) = \frac{8\pi n^2 \nu^2}{c^2} \frac{1}{e^{(h\nu-\mu)\beta} - 1} \quad (3)$$

where,  $n$  is the refractive index,  $\nu$  is the frequency,  $\mu$  is the photon chemical potential,  $\beta = 1/kT$ , and the other quantities have their usual meaning. The incident radiation,  $I_i$ , is not distributed over the same angular range as the escaping luminescence and thus must be treated separately. If  $I_i$  is incident at  $\theta_i$  it generates escaping fluxes,  $I_d^{(\pm)}$ , within the slab which depend only on  $z$  and the transmission angle,  $\theta_i$ :

$$\mp \frac{\partial I_d^{(\pm)}}{\partial z} = \frac{N\sigma_a}{\cos\theta_i} I_d^{(\pm)} \quad (4)$$

#### 4.1 Trapped fluxes

Suitable transparent media generally have refractive indices close to 1.5. Thus, the solid angle of totally trapped radiation  $\Omega_6 = 4\pi - 6\Omega_c$  is small. The trapped fluxes also equilibrate within the slab by multiple reflections and hence for a concentrator slab we may integrate the radiative transfer equation over this solid angle to obtain an average trapped intensity [5].

For a module, we need to apply boundary conditions at the right-hand surface to the trapped flux propagating in the positive  $x$  direction contained in the solid angle  $\Omega_6/2$  that take into account the presence of the solar cell bonded to that surface. Integrating the radiative transfer equation over the trapped solid angles  $\Omega_6/2$  in the positive and negative  $x$  directions also leads to two differential equations for the luminescent trapped fluxes  $I_t^{(+)}$  and  $I_t^{(-)}$ :

$$\mp \frac{\partial I_t^{(\pm)}}{\partial x} = \lambda_{at} I_t^{(\pm)} - \frac{\Omega_6}{8\pi} \lambda_{et} B \quad (5)$$

In Eqn. 5,  $\lambda_{at}$  and  $\lambda_{et}$  are defined by:

$$\lambda_{a,et} = \frac{N\sigma_{a,e} \left[ 2\pi - 12\pi \sin^2\left(\frac{\theta_c}{2}\right) \right]}{\pi - 4\theta_c + 2\sin 2\theta_c - \pi \sin^2 \theta_c} \quad (6)$$

#### 4.2 Detailed balance

The principle of detailed balance within the slab containing the luminescent species of quantum efficiency  $Q_e$  is used to determine the variation of  $\mu$  with position as in [5,6].  $I_C$ , the concentrated photon field within the slab [5] is obtained by adding the total trapped and escaping intensities in the  $x$ ,  $y$  and  $z$  directions:

$$I_C = I_x + I_y + I_z + I_d + I_t \quad (7)$$

The escaping intensities are themselves given by adding the appropriate fluxes as in Eqn. 8

$$I_{x,y,z,d,t} = I_{x,y,z,d,t}^{(+)} + I_{x,y,z,d,t}^{(-)} \quad (8)$$

#### 4.3 Boundary conditions

For the luminescent escaping fluxes,  $I_{x,y,z}^{(\pm)}$ , we have to consider reflection and transmission at the surfaces. For example, at the left surface  $x = 0$ , the far surface  $y = 0$  and the top surface  $z = 0$  these are:

$$I_{x,y,z}^{(+)}(0) = R_{L,F,T} I_{x,y,z}^{(-)}(0) \quad (9)$$

where,  $R_{L,F,T}$  are the appropriate reflection coefficients for the luminescent escaping fluxes at the left, far and top surfaces respectively. For a mirrored surface the reflection coefficient is independent of the angle of incidence but, for a bare surface it has a strong angular dependence and the appropriate reflection coefficients are calculated by averaging the results of the Fresnel formulae for the slab/air interface over the escape cone.

Similar boundary conditions on  $I_{x,y,z}^{(\pm)}$  apply at the right surface  $x = L$ , the near surface  $y = W$  and bottom surface  $z = D$ , with appropriate reflection coefficients  $R_{R,N,B}$  at the right, near and bottom surfaces respectively. At the right surface the appropriate reflection coefficient is that of the slab/glue/cell interface averaged over the solid angle of the escape cone.

At the top and bottom we also have boundary conditions on the fluxes  $I_d^{(\pm)}$ :

$$I_d^{(+)}(0) = (1 - R_{Td}) I_1 + R_{Td} I_d^{(-)}(0) \quad (10)$$

$$I_d^{(-)}(D) = R_{Bd} I_d^{(+)}(D) \quad (11)$$

with reflection coefficients  $R_{Td}$  and  $R_{Bd}$  as required for the angle of incidence of the direct incident light again calculated using the Fresnel formulae.

At the right surface where the solar cell is bonded to the slab we assume that the glue has the same or higher refractive index than the slab material such that there is no trapping at  $x = L$ . Thus the boundary conditions on the trapped fluxes are:

$$I_t^{(+)}(0) = I_t^{(-)}(0) \quad (12)$$

$$I_i^{(-)}(L) = R_i I_i^{(+)}(0) \quad (13)$$

where the appropriate reflection coefficient  $R_i$  at the right surface is that of the slab/glue/cell interface averaged over the solid angle  $\Omega_6/2$ .

In the  $x$  and  $y$  directions at the left,  $L$ , and far,  $F$ , surfaces, the boundary conditions for the luminescent escaping fluxes outside the slab are:

$$I_{L,F} = (1 - R_{L,F}) I_{x,y}^{(-)}(0) \quad (14)$$

with similar equations at the near,  $N$ , top,  $T$ , and bottom,  $B$ , surfaces.

At the right surface the fluxes  $I_i^{(+)}$  and  $I_x^{(+)}$  may both propagate into the solar cell. However, only the component of the trapped flux propagating in the  $x$  direction may escape into the cell, the remainder being trapped by the surfaces in the  $y$  and  $z$  directions. Since we ignore the spatial dependence of the angular factors we sample  $I_i^{(+)}$  over the hemisphere and find that only half may escape leading to the boundary condition:

$$I_R = (1 - R_R) I_x^{(+)}(L) + \frac{(1 - R_L)}{2} I_i^{(+)}(L) \quad (15)$$

By integrating the differential equations for the fluxes over the slab volume, evaluating the resulting expressions at the surfaces and applying the boundary conditions, we derive the escaping and trapped intensities within the slab and the fluxes escaping the surfaces. In carrying out these calculations, we rewrite the reflectivities as:

$$R_p = e^{-\alpha_p} \quad \alpha_{pQ} = \frac{\alpha_p + \alpha_Q}{2} \quad (16)$$

where  $P, Q = L, R, F, N, T, B, Td, Bd, t$ .

#### 4.4 Intensities within the slab and exiting fluxes

The expressions for the luminescent escaping intensities within the slab propagating in the  $x$ ,  $y$  and  $z$  directions are related by symmetry. For example  $I_x$  is given by

$$I_x(x, y, z) = \frac{\Omega_c \lambda_e \cosh(\lambda_a x + \frac{\alpha_L}{2})}{2\pi \sinh(\lambda_a L + \alpha_{LR})} \int_0^L dx' \cosh[\lambda_a(L - x') + \frac{\alpha_R}{2}] B(x', y, z) - \frac{\Omega_c \lambda_e}{2\pi} \int_0^x dx' \sinh[\lambda_a(x - x')] B(x', y, z) \quad (17)$$

and the expressions for  $I_y$  and  $I_z$  are generated by replacing the co-ordinate, the slab dimension and the  $\alpha$  subscripts in Eqn. 17 with those appropriate for the direction of interest. The intensity,  $I_d$ , within the slab owing to unabsorbed incident radiation is given by

$$I_d(z) = \frac{2I_1 \sinh(\frac{\alpha_{Td}}{2}) \cosh[\frac{N\sigma_a(D-z) + \alpha_{Bd}}{2}]}{\sinh(\frac{N\sigma_a D}{\cos\theta_i} + \alpha_{Td Bd})} \quad (18)$$

The final intensity required to solve the detailed balance [5,6] is the trapped intensity, given by:

$$I_i(x, y, z) = \frac{\Omega_6 \lambda_{et} \cosh(\lambda_a x)}{4\pi \sinh(\lambda_a L + \frac{\alpha_L}{2})} \int_0^L dx' \cosh[\lambda_a(L - x') + \frac{\alpha_L}{2}] B(x', y, z) - \frac{\Omega_6 \lambda_{et}}{4\pi} \int_0^x dx' \sinh[\lambda_a(x - x')] B(x', y, z) \quad (19)$$

The expressions for the luminescent fluxes outside the slab escaping the surfaces in the  $x$ ,  $y$  and  $z$  directions are again related by symmetry. For example the fluxes  $I_N$  and  $I_F$  escaping the near and far surfaces are:

$$I_N(x, z) = \frac{\Omega_c \lambda_e e^{-\alpha_{FN}} e^{-\lambda_a W} \sinh(\frac{\alpha_N}{2})}{2\pi \sinh(\lambda_a W + \alpha_{FN})} \int_0^W dy' \cosh[\lambda_a(W - y') + \frac{\alpha_N}{2}] B(x, y', z) + \frac{\Omega_c \lambda_e e^{-\frac{\alpha_N}{2}} \sinh(\frac{\alpha_N}{2})}{2\pi} \int_0^W dy' e^{-\lambda_a(W - y')} B(x, y', z) \quad (20)$$

$$I_F(x, z) = \frac{\Omega_c \lambda_e \sinh(\frac{\alpha_F}{2})}{2\pi \sinh(\lambda_a W + \alpha_{FN})} \int_0^W dy' \cosh[\lambda_a(W - y') + \frac{\alpha_N}{2}] B(x, y', z) \quad (21)$$

The expressions for  $I_L$  and the luminescent escaping components of  $I_B$ ,  $I_T$  and  $I_R$  are generated by appropriate substitution as for Eqn. 17. The fluxes escaping the top and bottom surfaces,  $I_B$  and  $I_T$ , contain additional terms arising from the incident flux  $I_1$  as described in [5].

The flux propagating into the solar cell at the right surface,  $I_R$ , also contains an additional term arising from the trapped flux  $I_i^{(+)}$ :

$$I_R(\text{trapped}) = \frac{\Omega_6 \lambda_{et} e^{-\frac{\alpha_L}{2}} e^{-\lambda_a L} \sinh(\frac{\alpha_L}{2})}{8\pi \sinh(\lambda_a L + \frac{\alpha_L}{2})} \int_0^L dx' \cosh[\lambda_a(L - x') + \frac{\alpha_L}{2}] B(x', y, z) + \frac{\Omega_6 \lambda_{et} e^{-\frac{\alpha_L}{2}} \sinh(\frac{\alpha_L}{2})}{8\pi} \int_0^L dx' e^{-\lambda_a(L - x')} B(x', y, z) \quad (22)$$

The intensities comprising  $I_C$  within the slab are calculated as outlined above by determining the chemical potential,  $\mu(x, y, z)$ , over a mesh of positions within the slab by Newton-Raphson iteration as in [5].

## 5 RESULTS

The frequency dependence of  $\sigma_c(\nu)$  at threshold for QDs with  $\delta$ -function density of states and Gaussian distributed diameters [3] is expected to be Gaussian. A Gaussian fits the experimental absorption very well down to threshold [5,6], and the calculated fluxes escaping the right surface for a slab of CdSe/CdS core-shell QDs in acrylic are illustrated in Fig. 1 for both a slab and a module which also shows the observed luminescence escaping the right surface of the slab.

Fig. 1 shows both the concentration of radiation into the flux collected by a solar cell at the right surface and the excellent agreement between the shape and position of the predicted and observed luminescence. It also shows the gain in the escaping flux,  $I_R$ , when a solar cell is bonded to the right face. Since there is less trapping in

such a module compared to a slab more radiation may escape the right surface and, in addition, this leads to both a lower concentrated intensity  $I_C$  and photon chemical potential  $\mu$ . This allows the module to radiate lower energy photons compared to the slab leading to the slightly larger red-shift.

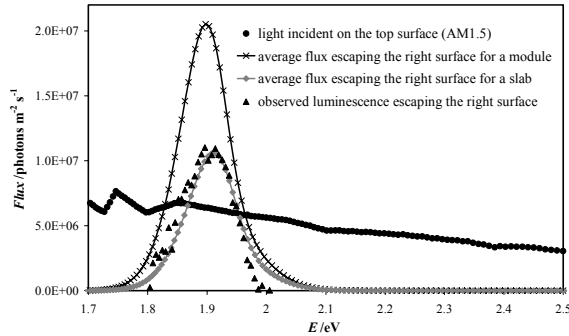


**Fig. 1** Predicted average fluxes escaping the right surfaces of a slab and module ( $L \times W \times D = 42 \times 10 \times 5 \text{ mm}$ ) of CdSe/CdS QDs with  $Q_e = 0.5$  in acrylic together with the normalised observed luminescence escaping the right surface of the slab. The module has a BP Si concentrator cell bonded to the right face with sil-gel and both it and the slab are illuminated by AM1.5 at normal incidence.

### 5.1 Photocurrent measurements

Short circuit currents,  $J_{sc}$ , resulting from the radiation escaping the right surfaces of various slabs and modules were measured and are compared with the predicted values in Table I. Measurements were performed on a slab of CdSe/CdS QDs in acrylic, a slab of red dye in perspex, a mirrored slab of red dye in perspex and a module comprising a slab of red dye in perspex with a BP silicon concentrator cell bonded to the right face with sil-gel. The mirrored slab had aluminium evaporated onto the left, near, far and bottom surfaces.

**Table I.** Measured and predicted short circuit currents,  $J_{sc}$ , for the slabs and module investigated.

Slab/Module	Slab Size /mm	$Q_e$	$J_{sc}/\text{mA m}^{-2} @ x = L$	
			Exp	Pred
CdSe/CdS QD slab	42×10×5	0.50	11.1±2.0	10.0±1.4
Red dye slab	40×15×3	0.95	20.1±2.0	22.1±1.7
Mirrored red dye slab	40×15×3	0.95	26.0±2.0	26.2±2.6
Red dye module	40×15×3	0.95	31.1±2.0	29.3±2.8

The slabs were positioned on a matt black stage with a matt black background to avoid unwanted reflections and were illuminated at normal incidence by a calibrated tungsten halogen lamp. A 2.65×2.65mm Siemens silicon solar cell, which could be positioned against any surface, was used to obtain  $J_{sc}$  values for the slabs. The uncertainty in the measurements is due to current generated by coupling of the incident light into the edges of the solar cell. Allowance has been made for this by background measurements. The uncertainty in the predictions is due to the 5% uncertainty in the absorption.

In these calculations we assume that the reflectivity of the evaporated aluminium mirrors is 0.9 and that the BP silicon concentrator cell which has an anti-reflection coating and a textured surface gives a reflectivity of 0.05 for the slab/sil-gel/cell interface in the module.

It is very encouraging that all the measurements agree so well with the predictions given that the materials have very different losses owing to the high  $Q_e$  of the dye and relatively low  $Q_e$  of the QDs. Our confidence in the models is also increased by the agreement with experiment for the slab with mirrored surfaces and the continued agreement seen for the module.

## 6 CONCLUSIONS

We have developed self-consistent thermodynamic models for planar solar concentrators and modules which allow for overlap of the incident radiation with the luminescence, for reflections at the surfaces, for re-absorption and for absorption losses in the host material. Our 3D flux models were derived by applying the method of Schwarzschild and Milne to Chandrasekhar's general radiative transfer equation coupled to a detailed balance condition. We can predict the efficiencies of luminescent concentrators using only the absorption properties of the slab, its refractive index, and the  $Q_e$  of the luminescence. To predict the efficiencies of modules we also require the QE of the solar cell and the reflectivity of the slab/glue/cell interface. The QD size distribution can be chosen to *minimise* the overlap between absorption and luminescence, which is a significant advantage for the QDC compared with the dye concentrator. Our results show that the 3D flux models can predict both the red-shift and profile of the luminescence as well as the total flux escaping each surface providing a tool for optimisation of the QDC and modules.

### ACKNOWLEDGEMENT

This work has been made possible in part by the sixth framework program European Commission Integrated Project FULLSPECTRUM contract no. SES6-CT-2003-502620.

### REFERENCES

- [1] A. Goetzberger and W. Greubel, *Appl. Phys.* **14** (1977) 123.
- [2] A. Goetzberger, W. Stahl and V. Wittwer, *Proceedings of the 6<sup>th</sup> European Photovoltaic Solar Energy Conference*, (Reidel, Dordrecht, 1985) 209.
- [3] K. W. J. Barnham, J. L. Marques, J. Hassard and P. O'Brien, *Appl. Phys. Lett.* **76** (2000) 1197.
- [4] A. P. Alivisatos, *MRS Bulletin*, **February** (1998) 18.
- [5] A. J. Chatten, K. W. J. Barnham, B. F. Buxton, N. J. Ekins-Daukes and M. A. Malik, *Proceedings of the 3<sup>rd</sup> World Conference on Photovoltaic Energy Conversion*, (Osaka, Japan, 2003) on CD.
- [6] A. J. Chatten, K. W. J. Barnham, B. F. Buxton, N. J. Ekins-Daukes and M. A. Malik, to be published in *Semiconductors* (2004).
- [7] E. A. Milne, *Monthly Notices Roy. Astron. Soc. London* **81** (1921) 361.
- [8] S. Chandrasekhar, "Radiative Transfer", (Clarendon, Oxford, UK, 1950).
- [9] E. Yablonoitch, *J. Opt. Soc. Am.* **70** (1980) 1362.